RSC Advances

Hybrid core-shell nanostructured electrodes made of polypyrrole nanotubes coated with Ni(OH)2 nanoflakes for high energy-density supercapacitors

Journal:	*RSC Advances*
Manuscript ID	Draft
Article Type:	Paper
Date Submitted by the Author:	n/a
Complete List of Authors:	Wolfart, Franciele ; Universidade Federal do Paraná, Departamento de Química Dubal, deepak; Gwangju Institute of Science and Technology, School of Materials Science and Engineering Vidotti, Marcio; Universidade Federal do Parana (UFPR), Química Gomez-Romero, Pedro; Nanoscience and Nanotechnology Research Center (CSIC-ICN),
Subject area & keyword:	Electrochemical energy < Energy

Hybrid core-shell nanostructured electrodes made of polypyrrole nanotubes coated with $Ni(OH)_2$ nanoflakes for high energy-density supercapacitors

Franciele Wolfart,[a] *Deepak P. Dubal,*[b]* *Marcio Vidotti,*[a] *Pedro Gómez-Romero,*[b]**

[a]Grupo de Pesquisa em Macromoléculas e Interfaces, Departamento de Química, Universidade Federal do Paraná, CP 19032, 81531-980, Curitiba, PR, Brazil.

[b]Institut Català de Nanociència i Nanotecnologia, ICN2 (CSIC-CERCA), Campus UAB, 08193 Bellaterra, Barcelona, Spain.

Corresponding author foot note

Prof. Pedro Gómez-Romero and Dr. Deepak P. Dubal,

Tel.: +349373609/+345929950 Fax: +345929951

E-mail: pedro.gomez@cin2.es (P. Gomez-Romero)

dubaldeepak2@gmail.com (D. P. Dubal)

Abstract

This work describe the design of $Ni(OH)_2$@PPy-NTs core-shell nanostructures with potential application as electrode material for supercapacitors. Initially, one dimensional (1D) polypyrrole nanotubes (PPy-NTs) were synthesized through chemical oxidation mediated soft template-directed route using anions azo dye methyl orange (MO). Subsequently, three dimensional (3D) $Ni(OH)_2$ nanoflakes were grown onto PPy-NTs by a simple hydrothermal route. This exclusive $Ni(OH)_2$@PPy-NTs nano-architecture helps to improve the overall electrochemical performance of the electrode, due to the high surface area provided by 3D nanoflakes and excellent electronic/ionic conductivity of 1D nanotubes. The maximum specific capacitance obtained for $Ni(OH)_2$@PPyNTs was 536 F g^{-1} with specific energy and power of 12 Wh kg^{-1} and 3.7 kW kg^{-1}, respectively. Last but not least, EIS technique showed low electrochemical series resistance for $Ni(OH)_2$@PPy-NTs confirming their promise as high-performance energy storage material.

Keywords: Core-shell nanostructures, PPy nanotubes, supercapacitors, nickel hydroxide.

Introduction

The continuous increase in the use of portable electronic devices and the emergence of new markets like the one of electric vehicles strongly calls for ever more reliable electric energy storage systems. Among different existing storage systems, supercapacitors have attracted widespread research interest because of their high power density, fast recharge capability and long cycle life [1]. When reversible faradaic redox reactions are introduced at the electrode/electrolyte interfaces, a pseudocapacitor electrode is formed, which has capacitance considerably exceeding than that of carbon based supercapacitors based on electrical double-layer charge storage [2]. That's why, transition metal oxides with variable valence have been extensively investigated for supercapacitors in view of their multiple oxidation states for pseudocapacitance contribution. However, due to the intrinsically poor electrical conductivity of metal oxides/hydroxides and the short diffusion distance of electrolytes into electrodes, only the exposed surface of electroactive materials can effectively contribute to the total capacitance leading to lower satisfactory parameters [3]. Hence, it is a great challenge to boost the electrochemical utilization of active materials by rationally designing electrodes with novel nanostructures.

An emerging attractive concept is to fabricate core-shell nanostructure with the combination of two types of materials and/or nanostructures. This is the easiest way to enhance accessible electroactive sites, shorten ion transport pathways, increase the electron collection efficiency, and even attractive synergetic properties of components simultaneously achieved to deliver high capacitance, excellent cycling life and rate performance.

Truly, the development of core-shell nanostructures with two different materials and two different nanostructures is a great design approach which can combine physical/chemical properties of materials as well as nanostructures [4]. The materials used can be organic or inorganic both core and shell, or mixed combinations [4,5]. Controlling the shell-thickness and the core-size is possible to modify the properties, generating a versatility of applications of

these systems [6] such as energy storage devices, solar cells, photochromic devices, biomedical applications, including, drug carriers for controlled drug release [7,8].

Aiming towards the fabrication of high performance supercapacitive electrodes, we chose polypyrrole (PPy) nanotubes as core material whereas $Ni(OH)_2$ nanoflakes was targeted as shell material in order to form $Ni(OH)_2$@PPy core-shell nanostructures. Both materials are from different families and chemistries but they are both strong contenders as supercapacitive electrode materials. Among different conducting polymers, PPy is one of the most widely investigated. It possesses high electrical conductivity and good environmental stability compared to other conductive organic polymers due to its unique π-stacked co-planar structure in solid state assisted by π-π conjugation interaction [9]. Whereas, $Ni(OH)_2$ is a classical material to modify electrodes, the $Ni(OH)_2$/NiOOH redox pair has remarkable properties that have been successfully applied in secondary batteries, electrocatalysis and electrochromism [10-13]. Two different polymorphs are possible to begin with (β-$Ni(OH)_2$ and α-$Ni(OH)_2$) characterized by the orientation along *c* axis [13]. The capability to energy storage and stability of the electrode is associated to the polymorph structure.

Herein, we present the synthesis of unique ($Ni(OH)_2$@PPy) core-shell nanostructures in which 3D $Ni(OH)_2$ nanoflakes grow as a 'shell' onto polypyrrole nanotubes which constitute the 'core' material in order to fabricate high performance supercapacitor electrode. To begin with, polypyrrole nanotubes (PPy-NTs) were synthesized through chemical oxidation mediated soft template-directed route. Subsequently, $Ni(OH)_2$ nanoflakes were grown onto PPy-NTs by a simple and cost-effective hydrothermal route. These nanostructures were characterized by different techniques in order to get clear insights about structure, morphology, surface area etc. The electrochemical properties were investigated by cyclic voltammetry (CV), galvanostatic charge/discharge and electrochemical impedance techniques in 6 mol L^{-1} KOH electrolyte.

Experimental section

Synthesis of PPyNTs

PPyNTs were prepared using the procedure described in the literature [14]. Briefly, 0.15 mmol MO (sodium 4-[(4-dimethylamino)phenyldiazenyl]benzenesulfonate) and 1.5 mmol $FeCl_3$ were dissolved in 30 ml deionized water (Milli Q, 18 MΩ resistance), which will turn in a flocculent precipitate immediately. Then, 1.5 mmol pyrrole (Py) freshly distilled was added to the above solution, followed by stirring at room temperature for 24 h. The formed precipitate was filtered-off and repeatedly washed with mixture of deionized water and ethanol and dried overnight under vacuum at 70 °C.

Synthesis of $Ni(OH)_2$

Nickel hydroxide ($Ni(OH)_2$) was prepared by hydrothermal synthesis. To do so, ammonium hydroxide (NH_4OH) 35 % (from Fluka) was dropped slowly at 50 mL of 0.1 mol L^{-1} nickel nitrate solution to maintain pH around 12. Then, the reaction mixture was transferred to a Teflon-lined stainless steel autoclave and heated at 80 °C for 7 h. The precipitate formed was collected by filtration, washed with deionized water and ethanol several times and finally dried overnight under vacuum at 70 °C.

Synthesis of nanocomposite $Ni(OH)_2$@PPyNTs

Important steps involved in the synthesis of $Ni(OH)_2$@PPy core-shell nanostructure are schematically shown in Fig. 1. First, 0.1mg mL^{-1} PPyNTs were dispersed in 25 mL of deionized water by ultra-sonication. Then, 25 mL of 0.1 mol L^{-1} $Ni(OH)_2$ precursor solution was added to the above solution. The mixture was sonicated for 30 min and stirred for 1 h in order to get a uniform dispersion. Finally, this whole solution was transferred to a Teflon-lined stainless steel autoclave and maintained at 80 °C for 7 h. At the end, the product was collected by filtration, washed with deionized water and ethanol several times and dried in vacuum oven at 70 °C overnight.

Material Characterization

Surface morphological analyses were carried out by scanning electron microscopy (FEI Quanta 650F Environmental SEM) and transmission electron microscopy (Tecnai G2 F20 S-TWIN HR(S) TEM, FEI). Structural properties were examined by powder X-ray diffraction (XRD) using Panalytical X'Pert Pro-MRD instrument (Cu Kα source (λ = 0.154). X-ray photoelectron (XPS) analysis was carried out by X-ray photoelectron spectroscopy (XPS, SPECS Germany, PHOIBOS 150). Fourier transform infrared (FTIR) spectra in a range of 4000-400 cm^{-1} were carried out with a Tensor 27/PMA 50 FTIR Spectrometer. N_2 adsorption/desorption was determined by Brunauer-Emmett-Teller (BET) measurements using Micromeritics instrument (Data Master V4.00Q, Serial#:2000/2400).

Electrode preparation and electrochemical testing

The working electrode was prepared by doctor blade method, by spreading through a moving blade onto a stationary substrate [15]. The pastes were prepared using 80 % of active material, 10 % of binder (PVDF) and 10 % of conducting material (carbon powder) in mass, dissolved in n-methylpyrrolidone (NMP). The supercapacitive performance of the materials was tested in 6 mol L^{-1} KOH using cyclic voltammetry (CV), galvanostatic charge/discharge (GCD) and electrochemical impedance techniques with conventional three electrode cell comprising a PPyNTs, $Ni(OH)_2$ or $Ni(OH)_2$@PPyNTs as a working electrode, platinum as a counter and Ag/AgCl as reference electrode, respectively. All electrochemical measurements were carried out with a Bio-Logic VMP3 Potentiostat.

Results and discussion

Fig. 2 (a and b) show the top-view field-emission scanning electron microscopy (FESEM) images of the PPy-NTs and $Ni(OH)_2$ samples, respectively. The PPy nanotubes are randomly spread with well-developed, highly open and porous structure on a large scale. No aggregation and alignment of bundles of PPy-NTs has been observed (Fig. 2a). Whereas $Ni(OH)_2$ exhibits irregular shaped micro-belts of random size (see Fig. 2b). In addition to this, we found the voids and pores between interconnected micro-belts and approximate length of the micro-belts is about 1-2 μm in range. Fig. 2 (c and d) show the typical FESEM images of final $Ni(OH)_2$@PPy-NTs core-shell nanostructures at two different magnifications. Clearly, no $Ni(OH)_2$ is packed in the interspace of the nanotubes, suggesting that $Ni(OH)_2$ nanoflakes are preferentially deposited onto the PPy nanotubes surface. Thus, the uniform coverage of $Ni(OH)_2$ nanoflakes on each PPy nanotube surface can be seen. Remarkably, even with two components integrated, the uniform 3D nanoflakes with 1D nanotubular structure are still well retained. Thus, nearly all the core-shell nanostructures are highly accessible to electrolytes for energy storage due to the presence of convenient diffusion channels.

In order to get more insights about the core-shell nanostructure, TEM analysis was carried out and is presented in Fig. 2 (e, f). As can be seen in the TEM image of the PPy-NTs (Fig. 2e), these nanotubes are highly porous and separated from each other. From Fig. 2f, it is evidently observed that the mesoporous PPy nanotubes (core material) is tightly bonded and totally covered with leaf-like thin $Ni(OH)_2$ nanoflakes, forming a typical core-shell hetero-structured architecture. Also, the TEM analysis further confirmed that the final nanostructure $Ni(OH)_2$@PPyNTs exhibits diameter of less than 200 nm (Fig. 2(f)).

Fig. 3(a) shows the XRD patterns of PPy-NTs, $Ni(OH)_2$ and $Ni(OH)_2$@PPy-NTs samples. It is interesting to note that, for PPy-NTs, a small hump is observed, corresponding to the repeat unit of pyrrole ring in PPy, implying the polymer chain is highly oriented. Whereas, XRD pattern for $Ni(OH)_2$ shows the polycrystalline nature with brucite-like hexagonal crystal

phase [13,16]. Moreover, the characteristic peak of 'β'- type $Ni(OH)_2$ at 19.35° corresponding to (001) plane along crystallographic *c* axis is also observed [17,18]. Strikingly, $Ni(OH)_2$@PPy-NTs exhibits the 'α'-type $Ni(OH)_2$ polymorph confirmed by the characteristic (001) peak at 12.39° [19,18]. It is well-known that, β-$Ni(OH)_2$ possesses more ordered structure along *c* axis, and it is the classic material used in battery system while α-$Ni(OH)_2$ exhibits more disordered structure as well as a larger separation distance between the layers than that of β-$Ni(OH)_2$, which can improve the electrochemical properties of the electrode and facilitate ion diffusion mechanism [18,20]. Moreover, the peak at 59° is characteristic of the hexagonal symmetry for both α and β polymorphs of $Ni(OH)_2$. The peak in the region between 30 to 45° is characteristic of the turbostratic disorder of the material [17]. The broadening of the peaks observed in the $Ni(OH)_2$@PPy-NTs composites may be attributed to the decrease of the hydroxide particles size and thus to the decrease of crystallite size upon PPy coating.

Fig. 3 (b) shows FTIR spectra of PPy-NTs, $Ni(OH)_2$ and $Ni(OH)_2$@PPy-NTs samples. The narrow and strong peak at 3632 cm^{-1} is assigned to hydroxyl groups stretching vibrations, which indicates the presence of free OH groups [21,22]. In addition, the peaks at 3578 cm^{-1} and 1630 cm^{-1} correspond to -OH stretching vibrations and water molecules intercalated in the lamellar $Ni(OH)_2$ structure, respectively. Two peaks at high frequencies 498 and 416 cm^{-1} are associated to (Ni–OH) bending vibration and the (Ni–O) stretching, respectively [22,23,21]. Furthermore, the characteristic peaks at 1540 and 1450 cm^{-1} are ascribed to the antisymmetric (C–N) and symmetric (C–C) stretching mode of the pyrrole ring. Additional peaks at 1296, 1031 and 963 cm^{-1} can be assigned to (=C–H) in and out plane and (C–C) in plane vibrations, respectively [24,25]. It is interesting to note that, a blue-shift is observed for (Ni–OH) bending vibration (630 cm^{-1}) and the peak around 3400 cm^{-1} (hydrogen-bonded) in case of $Ni(OH)_2$@PPyNTs hybrid which are characteristic of the α-$Ni(OH)_2$ phase, in good agreement with XRD analysis. Moreover, a slight shift from 1175 to 915 cm^{-1} and 1550 to 1430 cm^{-1} is observed for PPy-NTs [26].

Fig. 4 (a) shows the core-level XPS spectrum of Ni2p for $Ni(OH)_2$@PPy-NTs sample. The doublet of both transitions $Ni2p_{1/2}$ and $Ni2p_{3/2}$ between 850 to 890 eV are attributed to the presence of different oxidation states of Ni [27-29]. The characteristic peak at 857.68 is attributed to the presence of $Ni(OH)_2$. Biesinger *et al*. [27], correlates peak positions with the presence of β-$Ni(OH)_2$/NiOOH form, in higher ratio of NiOOH. In addition, two satellite peaks at 863.2 and 881.4 eV are also observed which are attributed to a sudden change in Coulombic potential when the photo-ejected electron passes through the valence band [30]. The obtained N1s peak in $Ni(OH)_2$@PPy-NTs sample corresponds to the characteristic nitrogen from PPy-NTs. The deconvolution of N1s peak gives three components as shown in Fig. 4 (b). The more intense component peak at 399.9 eV is attributed to the neutral N in the pyrrole ring (-NH) while the signals at high binding energies (401.1 eV) are attributed to the presence of oxidized states of the polypyrrole, known as polaron and bipolaron structures [31,32]. Also, the component peak at 398.2 eV could be ascribed to the π* character bonding from $C=N^+=C$ commonly found in "pyridinic" form [32]. The oxygen contributions (Fig. 4 (c)) are attributed to Ni-hydroxide (532.0 eV) [28], polymer oxidized (534.8 eV), water molecules intercalated in the material structure (533.7 eV) [8], and oxides (530.8) [30].

BET analysis was carried out in order to investigate the specific surface area of materials using N_2 adsorption/desorption analysis (see Fig. 5). The shape of the isotherms acquired for all materials show the hysteresis loop in relative pressure (P/P_0) between 0.6 to 1.0, showing characteristic of mesoporous materials [33]. The BET specific surface area obtained were 27.14, 43.18 and 77 m^2g^{-1} for $Ni(OH)_2$, PPyNTs and $Ni(OH)_2$@PPyNTs, respectively. Thus, the surface area of the PPy-NTs is higher than that of $Ni(OH)_2$, as expected for 1D nano-structures [34] while $Ni(OH)_2$@PPy-NTs exhibits remarkably larger specific surface area due to the synergetic combination of 1D nanotubes coated with 3D nanoflakes. Interestingly, $Ni(OH)_2$@PPy-NTs core-shell structure exhibits higher specific surface area than other core-shell structures. For example, $Ni(OH)_2$/CNT core-shell nanostructures deposited

onto nickel foams (0.819 m^2 g^{-1}) [35], TiO_2 nanotubes composite with PPy film (39 m^2 g^{-1}) [36] and comparable with PPy nanowires synthesized by alumina membrane template (75.66 – 172.90 m^2 g^{-1}) [37]. The increase of the specific surface area is directly associated to improvement of the supercapacitive properties of the materials, due to the mesoporous structures which enable the soaking of electrolyte, facilitating the ion diffusion and provide more electroactive sites for energy storage [33,38].

Electrochemical performance

Fig. 6 (a) displays the typical cyclic voltammetry (CV) curves of $Ni(OH)_2$, $Ni(OH)_2$@PPy-NTs and PPy-NTs at constant scan rate of 20 mV/s in KOH (6 moL L^{-1}). The shapes of CV curves for all three samples are different. In the case of PPy-NTs, the shape is quasi-rectangular reflecting the existence of purely capacitive (pseudo-capacitive) charge storing behavior [39,40]. Whereas, the CV curve for $Ni(OH)_2$ exhibits well-defined redox peaks which indicate that the capacity results mainly from a pseudo-capacitive behavior based on a redox (faradaic) mechanism. The appearance of anodic and cathodic peaks correspond to the $Ni(OH)_2$/NiOOH redox reaction[39,41,42]. The absence of a well-defined oxidation peak at the $Ni(OH)_2$ modified electrode is a clear evidence of the β-$Ni(OH)_2$ phase with lower electroactivity, as commented earlier. On the other hand, the $Ni(OH)_2$@PPy-NTs shows well-defined redox behavior with remarkable increase in current density, as denoted by the α-$Ni(OH)_2$ phase, corroborating the XRD and FTIR results. This considerable enhancement corresponds to $Ni(OH)_2$@PPy-NTs core-shell structures providing a substantially enhanced electrochemically active surface area as well as easy access to electrolyte ions. Moreover, for $Ni(OH)_2$@PPy-NTs composite, the redox peaks are more pronounced, suggesting an enhanced interaction at electrode/electrolyte interface which consequently improves their electrochemical properties [39,43].

In order to check the rate capability of electrode materials, CV curves at different scan rates were investigated and are presented in Fig. 6 (b-d). It is seen for all samples that the area under each curve increases with scan rate suggesting that the current density is directly proportional to scan rate. It is interesting to note that the shapes of CV curves of PPy-NTs even at high scan rates show good rate capability for this material (see Fig. 6 (b)). Further, the shapes of CV curves of $Ni(OH)_2$@PPy-NTs (Fig. 6(d)) and $Ni(OH)_2$ (Fig. 6(c)) are similar except that the redox process is more evidenced and the current density is higher for $Ni(OH)_2$@PPy-NTs (Fig. 6 (d)), due to the synergy between pseudo-capacitive $Ni(OH)_2$ and the highly conductive polymer nanotubes [40,44]. This excellent pseudo-capacitive behavior manifested in $Ni(OH)_2$@PPyNTs is due to the conversion from $Ni^{II}(OH)_2/Ni^{III}OOH$ present on the shell of the hybrid material. Moreover, it should also be noted that as the scan rate increases, the shape of the CV changes, the potential of the anodic and cathodic peaks shift to more positive and negative directions, respectively, and the capacitance inevitably decreases. It is worth noting that the performance and reversibility of $Ni(OH)_2$@PPy-NTs electrode at high scan rate is preserved, suggesting the effective utilization of active materials [39,45].

The electrochemical performance of the materials were also investigated by galvanostatic charge/discharge (GCD) tests at different current densities (2-20 mA cm^{-2}) and are displayed in Fig. 7. As seen in Fig. 7 (a), the shapes of CD curves are different for all three samples. It can be seen that all of the curves are not ideal straight lines, indicating the involvement of a faradaic reaction process. Furthermore, charging curves are not symmetric to its corresponding discharging counterpart. In addition, there is an initial drop in potential, which may be caused by the internal resistance as well as different rates of oxidation and reduction reactions. It is also noted that the discharging time of $Ni(OH)_2$@PPy-NTs sample is much longer than that of PPy-NTs and $Ni(OH)_2$ samples at identical current density conditions (Fig. 7 (a)).

Fig. 7 (b) shows the charge/discharge curves of $Ni(OH)_2$@PPy-NTs at different current densities. A low current density is used to allow for the complete reaction between the electrolyte and the electrode. The discharging time decreased with increasing current density, showing the redox reaction is a diffusion-controlled process. The nonlinearity and relatively slow charge/discharge process could be explained from contributions of faradaic reaction occurring at the material surface [39]. Monitoring discharge process is possible to assess the capacitance properties of the material. Specific capacitance values of $Ni(OH)_2$, PPy-NTs and $Ni(OH)_2$@PPy-NTs samples have been calculated from the voltage-time measurements (excluding internal resistance drop) at different applied current densities using the following equation:

$$C_s = \frac{i_D \times \Delta t_D}{m \times \Delta V} \quad (1)$$

where, C_s is specific capacitance, i_D is applied discharge current, Δt_D is discharge time, m is mass of the active material and ΔV is potential range. The masses of active material were 2.3, 1.06 and 0.35 mg cm^{-2} for $Ni(OH)_2$, $Ni(OH)_2$@PPy-NTs and PPy-NTs, respectively. The maximum specific capacitance obtained were 536, 201 and 115 F g^{-1} for $Ni(OH)_2$@PPyNTs, $Ni(OH)_2$, and PPyNTs, respectively. The specific capacitance decreases with the increase in current density, as expected which is attributed to delayed ion diffusion taking place when faster discharge is imposed to the material. Also the electrochemical kinetics is limited, which reduce the electrode efficiency at high current densities [39].

The specific energy as well as the specific power are fundamental parameters for the evaluation of materials application in devices [39,45]. Fig. 7 (d) shows the traditional Ragone's plot (specific energy *vs* specific power) for the materials developed in this work. The maximum specific energy and specific power obtained for $Ni(OH)_2$@PPyNTs were 11.91 Wh kg^{-1} and 3773 W kg^{-1}, respectively. This observation is quite promising in the context of utilizing $Ni(OH)_2$@PPy-NTs sample for fabricating electrodes in supercapacitor devices. The key to the superior performance of $Ni(OH)_2$@PPy-NTs sample is the availability of large amounts of

inner core surface in the form of 1D nanotubes as well as 3D nanoflakes as outer shell surface. Furthermore, it should be possible to improve the overall supercapacitance performance of $Ni(OH)_2$@PPy-NTs sample by employing organic and ionic liquid electrolytes.

Electrochemical impedance analysis was carried out to investigate the resistances involved in the overall system at room temperature and is presented in Fig. 8. The electrodes exhibit small equivalent series resistance (ESR) 0.06, 0.14 and 0.12 Ω for $Ni(OH)_2$, $Ni(OH)_2$@PPy-NTs and PPy-NTs, respectively. Moreover, charge transfer resistances were found to be 0.06, 0.03 and 0.13Ω, for $Ni(OH)_2$, $Ni(OH)_2$@PPy-NTs and PPy-NTs, respectively. Low ESR and charge transfer resistance reveals high conductivity for all samples. The frequency at which there is deviation from the semicircle is called as ‘‘knee frequency’’, which reflects the maximum frequency at which capacitive behavior is dominant, in other words, the capability of energy storage [39]. The “knee frequency” found for $Ni(OH)_2$, PPy-NTs and $Ni(OH)_2$@PPy-NTs were 1313, 602 and 2869 Hz, respectively.

The excellent electrochemical supercapacitive properties of the $Ni(OH)_2$@PPy-NTs core-shell structure may be attributed to the following factors: 1) PPy-NTs have a remarkable capability to improve their electroactive properties in a 1D nanostructure, with the quantum confinement effect in one dimension facilitating charge transfer by high electronic conductivity [46]; 2) In addition, the anisotropic morphology can provide fast ion exchange [47]; 3) The core-shell nanostructures result in higher improvement by the combination of $Ni(OH)_2$ redox characteristic with the polymer capacitive properties, especially in supercapacitors application [45,48,49] ; 4) Thus, the charge storage at the electrode/electrolyte interface combines the physical process (electrical double layer) and the reversible oxidation/reduction reaction, resulting in the so called hybrid supercapacitors [45]; 5) Last but not least, 1D nanotubular PPy core material and 3D $Ni(OH)_2$ nanoflakes shell material provide high surface area and orientation of the active materials, small size and porous nature [39,47,50] which increase active sites for energy store and facilitates ion diffusion.

Conclusion

In conclusion, a facile and scalable strategy has been developed to construct unique $Ni(OH)_2$@PPy-NTs core-shell heterostructured nanoarchitectures with high electrochemical performance for supercapacitors. As fabricated $Ni(OH)_2$@PPy-NTs electrode shows maximum specific capacitance of 536 F g^{-1} at 2 mA cm^{-2} current density which is almost five times larger than the corresponding values for the individual component materials. In addition, the maximum specific energy and specific power are found to be 11.91 Wh kg^{-1} and 3.773 kW kg^{-1}, respectively. Thin enhanced capacitive behavior is attributed to the unique hierarchical core-shell heterostructured nanoflakes@nanotubes configuration and the synergistic effects of the combined pseudocapacitive contributions from the mesoporous PPy-NTs core and $Ni(OH)_2$ nanoflakes shell layer. This work confirms the feasibility of rational design of advanced integrated electrode materials for high-performance supercapacitors.

Acknowledgments

The authors acknowledge the financial support of the CAPES Foundation, Ministry of Education of Brazil: Process BEX 3196/14-3. Authors appreciate the award to DPD with the support of the Secretary for Universities and Research of the Ministry of Economy and Knowledge of the Government of Catalonia and the Co-fund programme of the Marie Curie Actions of the 7th R&D Framework Programme of the European Union". Partial funding from Spanish Grant MAT2012-39199-C02-01, is acknowledged. ICN2 acknowledges support of the Spanish MINECO through the Severo Ochoa Centers of Excellence Program under Grant SEV-2013-0295.

References

[1] Simon P, Gogotsi Y 2008 Materials for electrochemical capacitors *Nat. Mater.* **7** 845-854

[2] Guan C, Li X, Wang Z, Cao X, Soci C, Zhang H, Fan HJ 2012 Nanoporous Walls on Macroporous Foam: Rational Design of Electrodes to Push Areal Pseudocapacitance *Adv. Mater.* **24** 4186-90

[3] Lu Z, Yang Q, Zhu W, Chang Z, Liu J, Sun X, Evans DG, Duan X 2012 Hierarchical Co_3O_4@Ni-Co-O Supercapacitor Electrodes with Ultrahigh Specific Capacitance per Area *Nano Res.* **5** 369-78

[4] Caruso F 2001 Nanoengineering of particle surfaces *Adv. Mater.* **13** 11-22

[5] Jang J, Oh JH 2003 Facile fabrication of photochromic dye-conducting polymer core-shell nanomaterials and their photoluminescence *Adv. Mater.* **15** 977-80

[6] Caruso F, Caruso RA, Mohwald H 1998 Nanoengineering of inorganic and hybrid hollow spheres by colloidal templating *Science* **282** 1111-14

[7] Marinakos SM, Brousseau LC, Jones A, Feldheim DL 1998 Template synthesis of one-dimensional Au, Au-poly(pyrrole), and poly(pyrrole) nanoparticle arrays *Chem. Mater.* **10** 1214-19

[8] Yuan C, Zhang L, Zhu S, Cao H, Lin J, Hou L 2015 Heterostructured core-shell $ZnMn_2O_4$ nanosheets@carbon nanotubes' coaxial nanocables: a competitive anode towards high-performance Li-ion batteries *Nanotechnology* **26** 145401

[9] Wang X, Yang C, Wang T, Liu P 2011 Praseodymium oxide/polypyrrole nanocomposites for electrochemical energy storage *Electrochim. Acta* **58** 193-202

[10] Cabanas-Polo S, Gonzalez Z, Sanchez-Herencia AJ, Ferrari B, Caballero A, Hernan L, Morales J 2015 Cyclability of binder-free beta-$Ni(OH)_2$ anodes shaped by EPD for Li-ion batteries *J. Eur. Ceramic Soc.* **35** 573-84

[11] Luo Z, Yin S, Wang K, Li H, Wang L, Xu H, Xia J 2012 Synthesis of one-dimensional beta-$Ni(OH)_2$ nanostructure and their application as nonenzymatic glucose sensors *Mater. Chem. Phys.* **132** 387-94

[12] Wolfart F, Lorenzen AL, Nagata N, Vidotti M 2013 Nickel/cobalt alloys modified electrodes: Synthesis, characterization and optimization of the electrocatalytical response *Sensors Actuat. B-Chem.* **186** 528-35

[13] Provazi K, Giz MJ, Dall'Antonia LH, de Torresi SIC 2001 The effect of Cd, Co, and Zn as additives on nickel hydroxide opto-electrochemical behavior *J. Power Sources* **102** 224-32

[14] Yang XM, Zhu ZX, Dai TY, Lu Y 2005 Facile fabrication of functional polypyrrole nanotubes via a reactive self-degraded template *Macromol. Rapid Comm.* **26** 1736-40

[15] Berni A, Mennig M, Schmidt H 2004 Doctor Blade. In: Aegerter M, Mennig M (eds) Sol-Gel Technologies for Glass Producers and Users. Springer US, pp 89-92

[16] Vidotti M, Torresi R, Cordoba de Torresi SI 2010 Nickel Hydroxide Modified Electrodes: A Review Study Concerning Its Structural And Electrochemical Properties Aiming The Application In Electrocatalysis, Electrochromism And Secondary Batteries *Quim. Nova* **33** 2176-86

[17] Faure C, Delmas C, Fouassier M 1991 Characterization Of A Turbostratic Alpha-Nickel Hydroxide Quantitatively Obtained From An $NiSO_4$ Solution *J. Power Sources* **35** 279-90

[18] Freitas M 2001 Nickel hydroxide powder for NiO center dot OH/Ni(OH)(2) electrodes of the alkaline batteries *J. Power Sources* **93** 163-73

[19] Begum SN, Muralidharan VS, Basha CA 2009 The influences of some additives on electrochemical behaviour of nickel electrodes *Int. J. Hydrogen Energy* **34** 1548-55

[20] Hall DS, Lockwood DJ, Bock C, MacDougall BR 2015 Nickel hydroxides and related materials: a review of their structures, synthesis and properties *The Royal Society* **471**

[21] Ramesh TN, Kamath PV 200) Synthesis of nickel hydroxide: Effect of precipitation conditions on phase selectivity and structural disorder *J. Power Sources* **156** 655-61

[22] Xu L, Ding Y-S, Chen C-H, Zhao L, Rimkus C, Joesten R, Suib SL 2008 3D Flowerlike α-Nickel Hydroxide with Enhanced Electrochemical Activity Synthesized by Microwave-Assisted Hydrothermal Method *Chem. Mater.* **20** 308-16

[23] Song Q, Tang Z, Guo H, Chan SLI 2002 Structural characteristics of nickel hydroxide synthesized by a chemical precipitation route under different pH values *J. Power Sources* **112** 428-34

[24] Ravichandran S, Nagarajan S, Kokil A, Ponrathnam T, Bouldin RM, Bruno FF, Samuelson L, Kumar J, Nagarajan R 2012 Micellar Nanoreactors for Hematin Catalyzed Synthesis of Electrically Conducting Polypyrrole *Langmuir* **28** 13380-86

[25] Wen Q, Pan X, Hu Q-x, Zhao S-j, Hou Z-f, Yu Q-z 2013 Structure–property relationship of dodecylbenzenesulfonic acid doped polypyrrole *Synth. Met.* **164** 27-31

[26] Jing S, Xing S, Yu L, Zhao C 2007 Synthesis and characterization of Ag/polypyrrole nanocomposites based on silver nanoparticles colloid *Mater. Lett.* **61** 4528-30

[27] Biesinger MC, Payne BP, Lau LWM, Gerson A, Smart RSC 2009 X-ray photoelectron spectroscopic chemical state quantification of mixed nickel metal, oxide and hydroxide systems *Surf. Interface Anal.* **41** 324-32

[28] Marchetti L, Miserque F, Perrin S, Pijolat M 2015 XPS study of Ni-base alloys oxide films formed in primary conditions of pressurized water reactor *Surf. Interface Anal.* **47** 632-42

[29] Lee SJ, Jun JH, Lee SH, Yoon KJ, Lim TH, Nam SW, Hong SA 2002 Partial oxidation of methane over nickel-added strontium phosphate *Appl. Catal. a-General* **230** 61-71

[30] Hall DS, Lockwood DJ, Poirier S, Bock C, MacDougall BR 2012 Raman and Infrared Spectroscopy of a and beta Phases of Thin Nickel Hydroxide Films Electrochemically Formed on Nickel *J. Phys. Chem. A* **116** 6771-84

[31] Sevilla M, Valle-Vigon P, Fuertes AB 2011 N-Doped Polypyrrole-Based Porous Carbons for CO_2 Capture *Adv. Funct. Mater.* **21** 2781-87

[32] Morant C, Torres R, Jimenez I, Sanz JM, Elizalde E 2009 Characterization of Nitrogen-Doped Carbon Nanotubes by Atomic Force Microscopy, X-ray Photoelectron Spectroscopy and X-ray Absorption Near Edge Spectroscopy *J. Nanosci. Nanotechno.* **9** 3633-38

[33] Dubal DP, Lee SH, Kim JG, Kim WB, Lokhande CD 2012 Porous polypyrrole clusters prepared by electropolymerization for a high performance supercapacitor *J. Mater. Chem.* **22** 3044-52

[34] Lu J, Lim SX, Sow CH 2015 A Focused Laser Beam: A Useful and Versatile Tool for 1D Nanomaterials Research: A Review *J. Mater. Science & Technology* **31** 616-29

[35] Tang Z, Tang C-h, Gong H 2012 A High Energy Density Asymmetric Supercapacitor from Nano-architectured Ni(OH)2/Carbon Nanotube Electrodes *Adv. Funct. Mater.* **22** 1272-78

[36] Gao Y, Ding K, Xu X, Wang Y, Yu D 2014 PPy film/TiO2 nanotubes composite with enhanced supercapacitive properties *Rsc Advances* **4** 27130-34

[37] Hassanzadeh N, Omidvar H, Tabaian SH 2012 Chemical synthesis of high density and long polypyrrole nanowire arrays using alumina membrane and their hydrogen sensing properties. *Superlattice. Microstruct.* **51** 314-23

[38] Kim Y, Kim JG, Noh Y, Kim WB 2015 An Overview of One-Dimensional Metal Nanostructures for Electrocatalysis. *Catal. Surv. Asia* **19** 88-121

[39] Kim BK, Sy S, Yu A, Zhang J 2015 Electrochemical Supercapacitors for Energy Storage and Conversion. In: Handbook of Clean Energy Systems. John Wiley & Sons, Ltd.

[40] Li P, Yang Y, Shi E, Shen Q, Shang Y, Wu S, Wei J, Wang K, Zhu H, Yuan Q, Cao A, Wu D 2014 Core-Double-Shell, Carbon Nanotube@Polypyrrole@MnO2 Sponge as Freestanding, Compressible Supercapacitor Electrode *Acs Appl. Mater. Interfaces* **6** 5228-34

[41] Bettini LG, Divitini G, Ducati C, Milani P, Piseri P 2014 Nickel nanoparticles effect on the electrochemical energy storage properties of carbon nanocomposite films *Nanotechnology* **25** 435401

[42] Dubal DP, Lee SH, Kim WB 2012 Sponge-like beta-$Ni(OH)_2$ nanoparticles: synthesis, characterization and electrochemical properties *J. Mater. Sci.* **47** 3817-21

[43] Lee JW, Ahn T, Soundararajan D, Ko JM, Kim J-D 2011 Non-aqueous approach to the preparation of reduced graphene oxide/alpha-$Ni(OH)_2$ hybrid composites and their high capacitance behavior. *Chem. Commun.* **47** 6305-07

[44] Pan L, Qiu H, Dou C, Li Y, Pu L, Xu J, Shi Y 2010 Conducting Polymer Nanostructures: Template Synthesis and Applications in Energy Storage *Int. J. Mol. Sci.* **11** 2636-57

[45] Dubal DP, Ayyad O, Ruiz V, Gomez-Romero P 2015 Hybrid energy storage: the merging of battery and supercapacitor chemistries *Chem. Soc. Rev.* **44** 1777-90

[46] Xia YN, Yang PD, Sun YG, Wu YY, Mayers B, Gates B, Yin YD, Kim F, Yan YQ 2003 One-dimensional nanostructures: Synthesis, characterization, and applications *Adv. Mater.* **15** 353-89

[47] Singh AK, Sarkar D, Khan GG, Mandal K 2013 Unique hydrogenated Ni/NiO core/shell 1D nanoheterostructures with superior electrochemical performance as supercapacitors *J. Mater. Chem. A* **1** 12759-67

[48] Wang H, Yi H, Chen X, Wang X 2014 Asymmetric supercapacitors based on nano-architectured nickel oxide/graphene foam and hierarchical porous nitrogen-doped carbon nanotubes with ultrahigh-rate performance *J. Mater. Chem. A* **2** 3223-30

[49] Dubal DP, Holze R, Gomez-Romero P 2014 Development of hybrid materials based on sponge supported reduced graphene oxide and transition metal hydroxides for hybrid energy storage devices *Sci. Rep.* **4** 7349

[50] Zheng Y-Q, Wang J-Y, Pei J 2015 One-dimensional (1D) micro/nanostructures of organic semiconductors for field-effect transistors *Sci. China Chem.* **58** 937-46

Figures Caption

Fig. 1 Scheme of the 1D core-shell nanostructures synthesis.

Fig. 2 SEM image of PPy-NTs (a), $Ni(OH)_2$ (b) and $Ni(OH)_2$@PPy-NTs (c-d). TEM images of $Ni(OH)_2$@PPy-NTs (e-f).

Fig. 3 (a) XRD patterns (b) FTIR spectra of PPy-NTs, $Ni(OH)_2$ and $Ni(OH)_2$@PPy-NTs samples.

Fig. 4 XPS spectra of $Ni(OH)_2$@PPy-NTs sample: (a) Ni 2p, (b) N 1s and (c) O 1s, respectively.

Fig. 5 Nitrogen adsorption/desorption isotherm of PPy-NTs (a), $Ni(OH)_2$ (b) and $Ni(OH)_2$@PPy-NTs (c).

Fig. 6 (a) CV curves of PPy-NTs, $Ni(OH)_2$ and $Ni(OH)_2$@PPy-NTs electrodes at 20 mV s^{-1} scan rate. CV curves at various scan rate from 2-50 mV s^{-1} of (b) PPy-NTs, (c) $Ni(OH)_2$ and (d) $Ni(OH)_2$@PPy-NTs in 6 mol L^{-1} KOH aqueous solution.

Fig. 7 (a) Galvanostatic charge-discharge curves of PPy-NTs, $Ni(OH)_2$ and $Ni(OH)_2$@PPy-NTs and (b) GCD curves of $Ni(OH)_2$@PPy-NTs at different current densities in 6 mol L^{-1} KOH aqueous solution. (c) Variation of specific capacitance with current density and (d) Plot of specific power versus specific energy of the PPy-NTs, $Ni(OH)_2$ and $Ni(OH)_2$@PPy-NTs samples.

Fig. 8 Nyquist plots of PPy-NTs, $Ni(OH)_2$ and $Ni(OH)_2$@PPy-NTs.

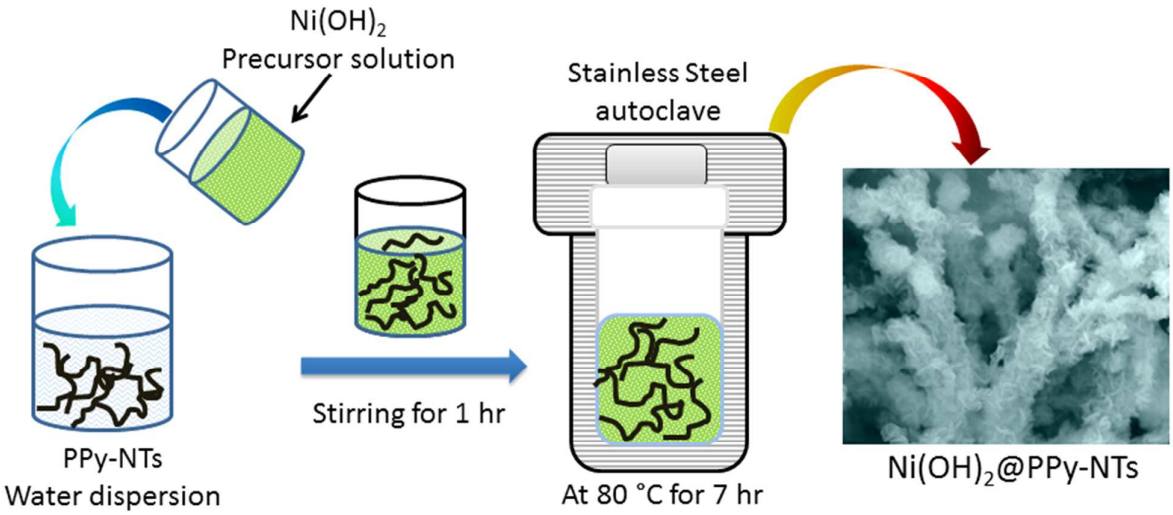
Ni(OH)2
Precursor solution
Stainless Steel
autoclave
PPy-NTs
Water dispersion
Stirring for 1 hr
At 80 °C for 7 hr
Ni(OH)2@PPy-NTs

Fig. 1

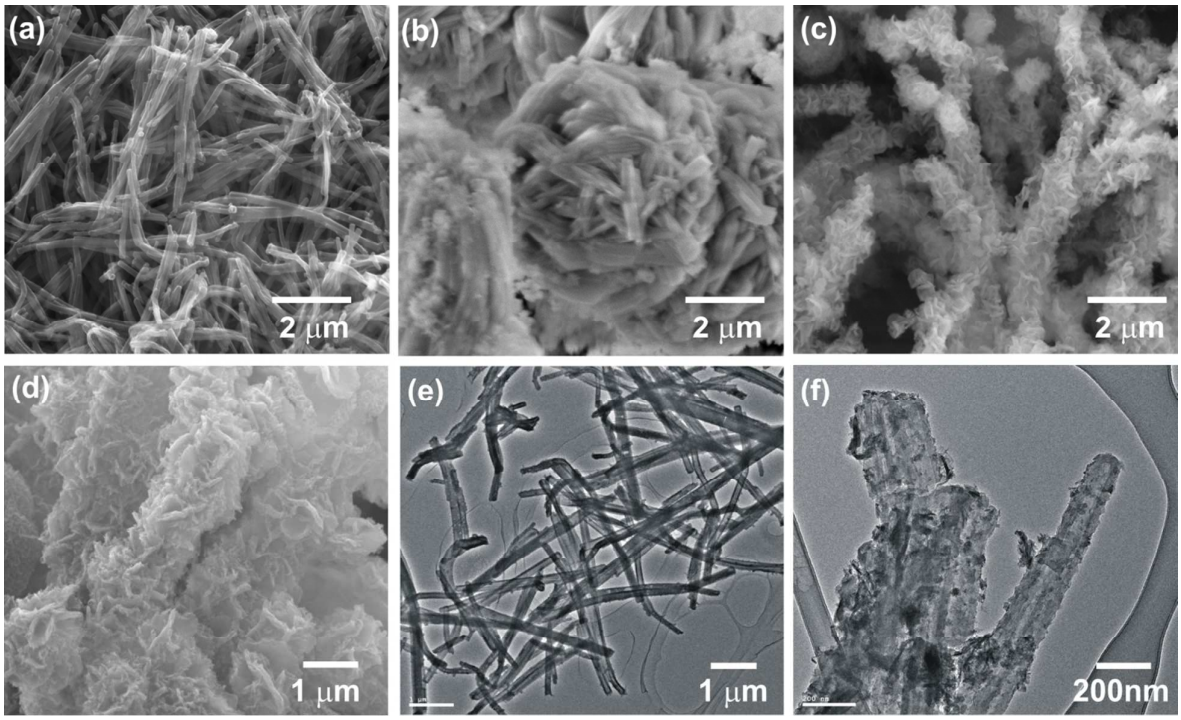

Fig. 2

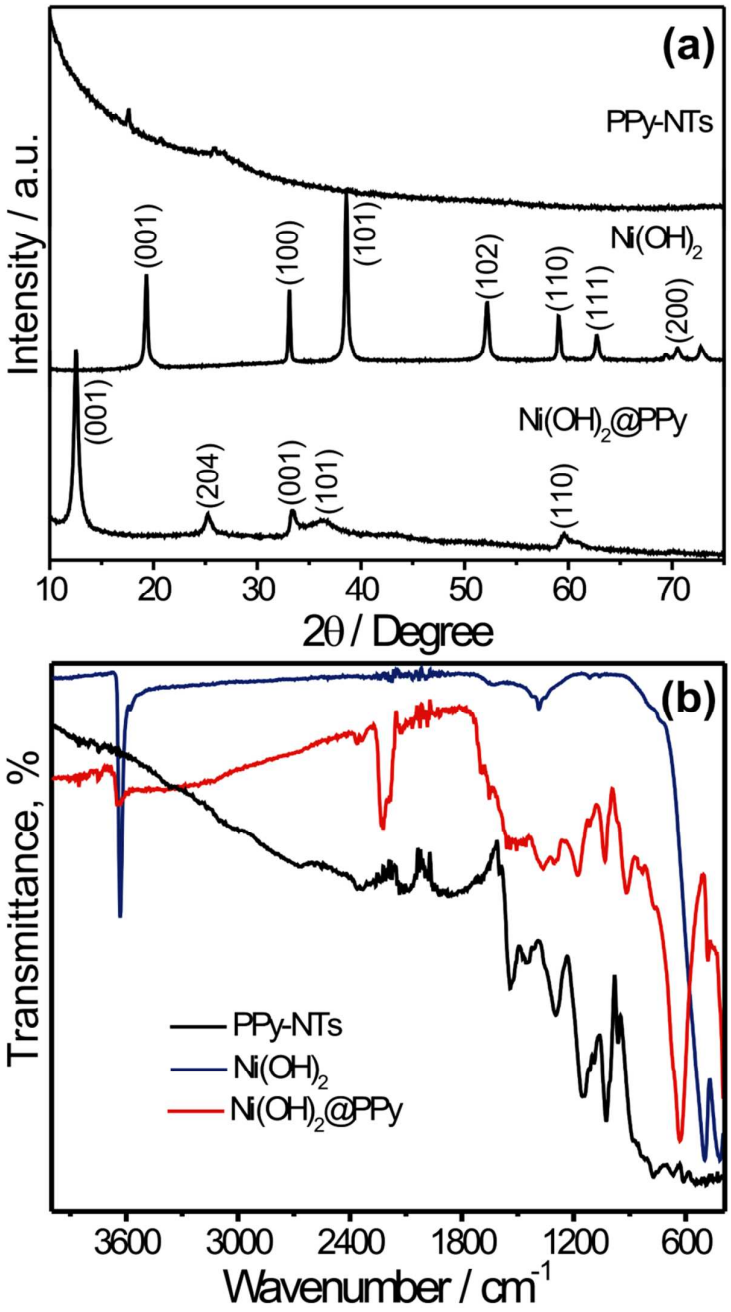
(a)
PPy-NTs
Ni(OH)2
Ni(OH)2@PPy
(001)
(100)
(101)
(102)
(110)
(111)
(200)
(001)
(204)
(001)
(101)
(110)
Intensity / a.u.
10
20
30
40
50
60
70
2θ / Degree
(b)
PPy-NTs
Ni(OH)2
Ni(OH)2@PPy
Transmittance, %
3600
3000
2400
1800
1200
600
Wavenumber / cm-1

Fig. 3

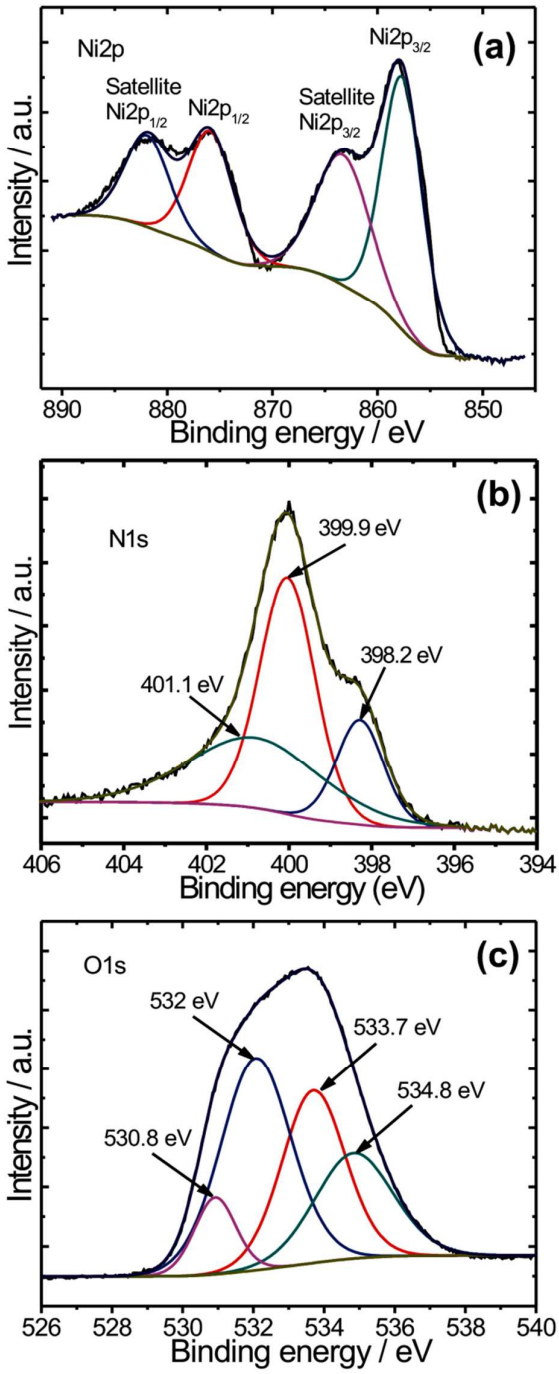
Ni2p
Satellite Ni2p1/2
Ni2p1/2
Satellite Ni2p3/2
Ni2p3/2
(a)
Intensity / a.u.
890 880 870 860 850
Binding energy / eV
N1s
399.9 eV
398.2 eV
401.1 eV
(b)
Intensity / a.u.
406 404 402 400 398 396 394
Binding energy (eV)
O1s
532 eV
533.7 eV
534.8 eV
530.8 eV
(c)
Intensity / a.u.
526 528 530 532 534 536 538 540
Binding energy / eV

Fig. 4

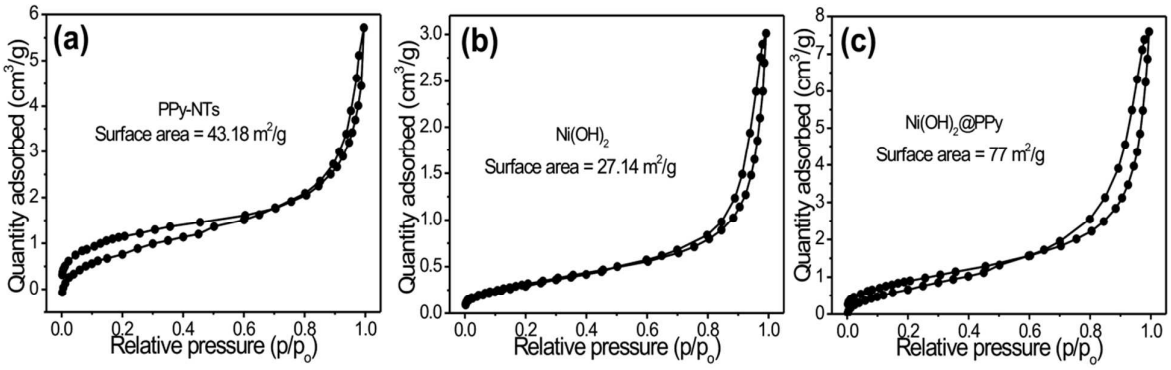
(a)
PPy-NTs
Surface area = 43.18 m²/g
Quantity adsorbed (cm³/g)
Relative pressure (p/p₀)
(b)
Ni(OH)₂
Surface area = 27.14 m²/g
Quantity adsorbed (cm³/g)
Relative pressure (p/p₀)
(c)
Ni(OH)₂@PPy
Surface area = 77 m²/g
Quantity adsorbed (cm³/g)
Relative pressure (p/p₀)

Fig. 5

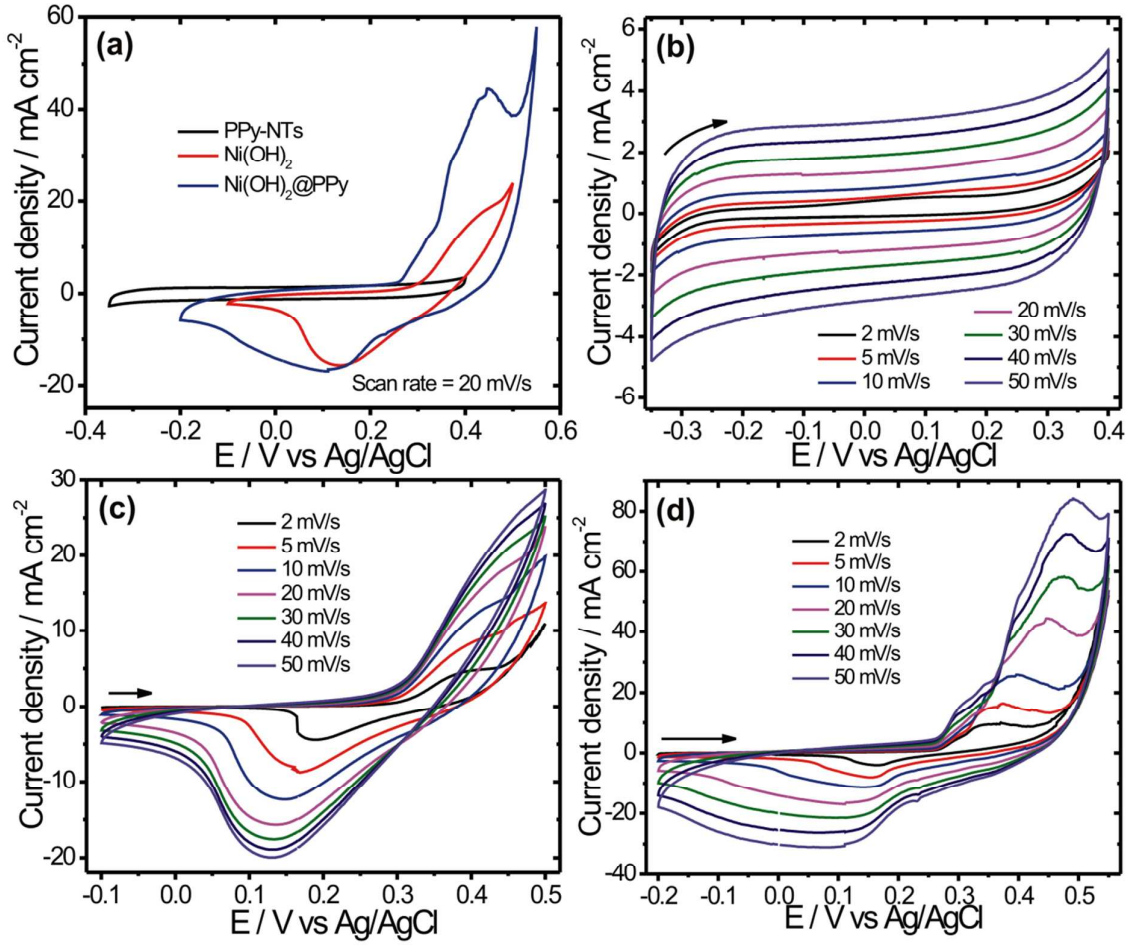
(a)
PPy-NTs
Ni(OH)2
Ni(OH)2@PPy
Scan rate = 20 mV/s
Current density / mA cm-2
E / V vs Ag/AgCl
(b)
2 mV/s
5 mV/s
10 mV/s
20 mV/s
30 mV/s
40 mV/s
50 mV/s
(c)
(d)

Fig. 6

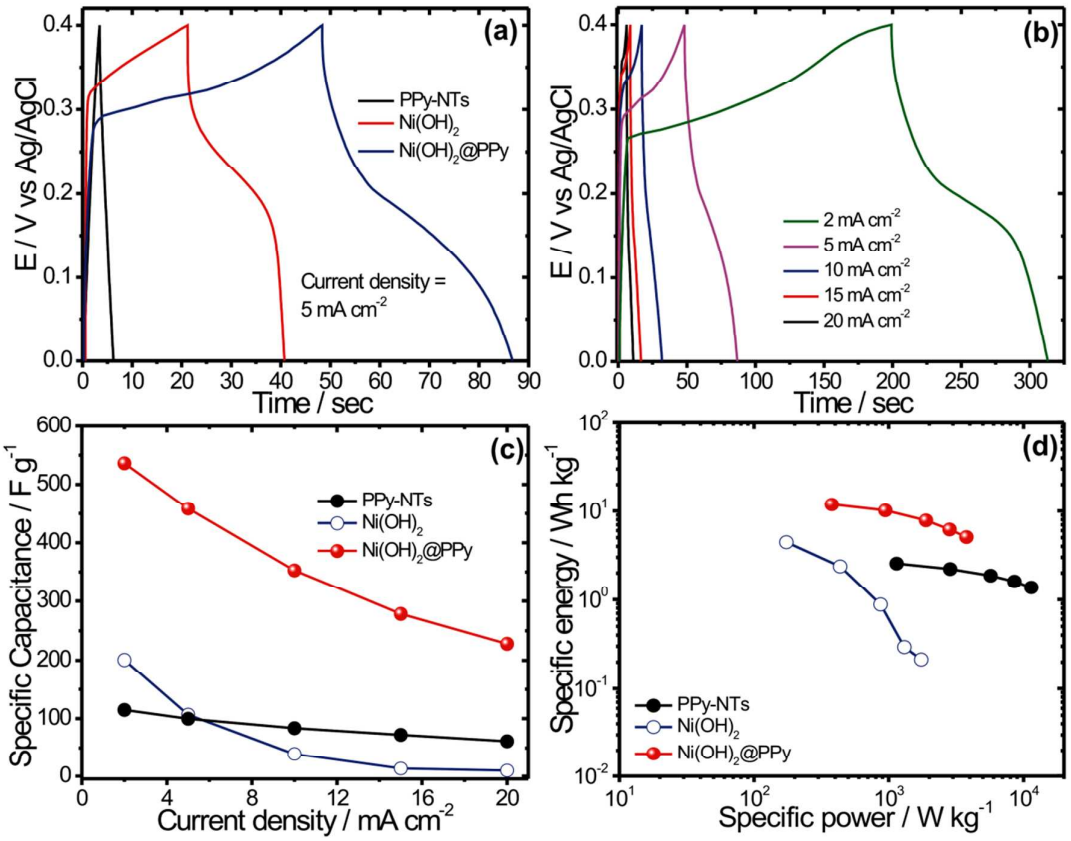
(a)
PPy-NTs
Ni(OH)2
Ni(OH)2@PPy
Current density =
5 mA cm-2
E / V vs Ag/AgCl
Time / sec
(b)
2 mA cm-2
5 mA cm-2
10 mA cm-2
15 mA cm-2
20 mA cm-2
E / V vs Ag/AgCl
Time / sec
(c)
PPy-NTs
Ni(OH)2
Ni(OH)2@PPy
Specific Capacitance / F g-1
Current density / mA cm-2
(d)
PPy-NTs
Ni(OH)2
Ni(OH)2@PPy
Specific energy / Wh kg-1
Specific power / W kg-1

Fig. 7

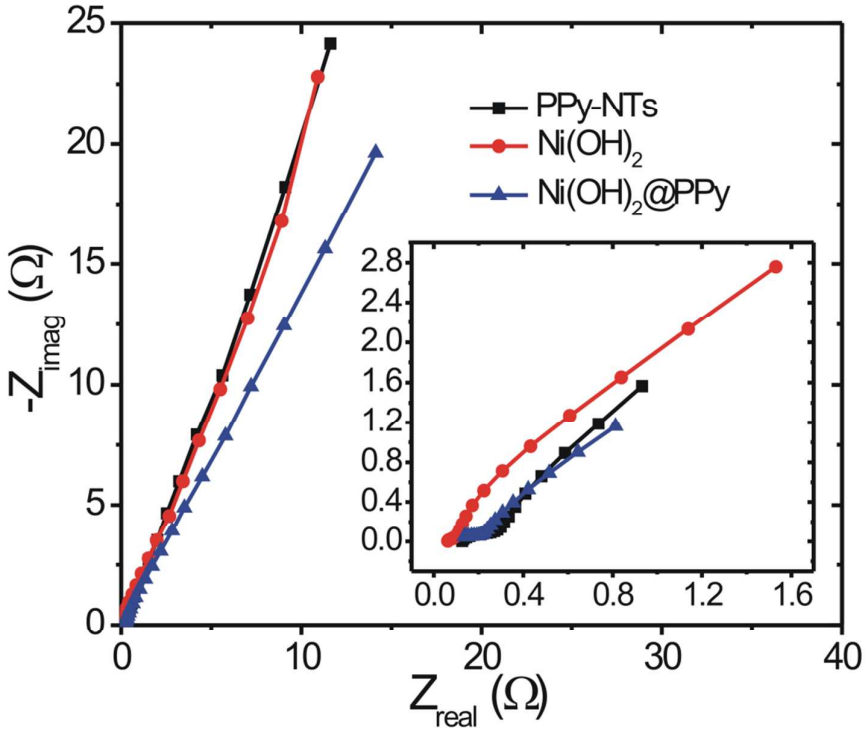
PPy-NTs
Ni(OH)2
Ni(OH)2@PPy
-Zimag (Ω)
Zreal (Ω)
0
5
10
15
20
25
0
10
20
30
40
0.0
0.4
0.8
1.2
1.6
2.0
2.4
2.8

Fig. 8

Graphical Abstract

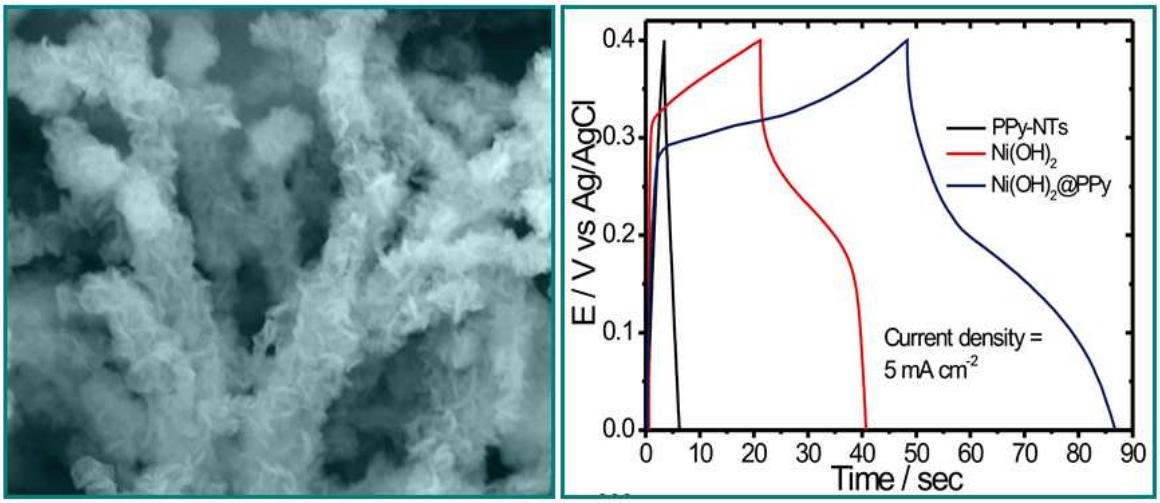

SEM image of Ni(OH)2@PPy core-shell nanostructure and galvanostatic charge/discharge curves of PPy-NTs, $Ni(OH)_2$ and $Ni(OH)_2$@PPy nanostructures